An Experimental Study of Instabilities and Other Flow Properties of a Laminar Pipe Jet

Flow patterns in an axisymmetrical laminar pipe jet with a flat entering velocity profile and a diametrical expansion ratio of 1:2 was investigated using nondisturbing flow visualization. A wavelike instability was discovered in the detached shear layer even at the lowest Reynolds numbers, and for Reynolds numbers greater than 350 tangential motions were observed, resulting in considerable turbulence near the mean position of re-attachment. This turbulence even at low Reynolds explains local high rates of mass and heat transfer. The mean re-attachment position depends on Reynolds number.

Instantaneous mean velocity profiles and wall shear stresses were determined.

AGRIPINA IRIBARNE
FRANTISEK FRANTISAK
RICHARD L. HUMMEL
JAMES W. SMITH

Department of Chemical Engineering
and Applied Chemistry
University of Toronto
Toronto 181, Ontario, Canada

SCOPE

Because of the experimental difficulties involved, few engineering studies of flow conditions at the entry and exit of pipe sections have been made. The abrupt expansions and contractions resulting from the installation of orifices, valves, pipe joints, etc. often result in flow separations and local recirculations which have an important effect on heat, mass, and momentum transfer.

Spalding and his group at London Imperial College have been developing general procedures for predicting heat and mass transfer for turbulent flows. Their equations consider not only total turbulent energy, but also vorticity, a basis which is a theoretical improvement and leads to additional constants or functions to be determined by experiment. Separated flow is an important regime for testing and developing the procedures, and the pipe jet, having axial symmetry, is an obvious choice for study. Runchal (1969) from Spalding's group studied the mass transfer experimentally and theoretically for this system and it was suggested by Spalding that the fluid dynamics be studied in Toronto using Hummel's (1967, 1969) technique. The fluid mechanics show a surprising degree of turbulence in the attachment region even at low Reynolds numbers, which may largely explain why the experimental mass transfer is much greater than the predicted mass transfer in this region.

The fluid mechanics, not only of the attachment region but also of the entire reverse flow region, can be studied using the nondisturbing flow visualization technique. The method consists of dissolving a photochromic dye in the test fluid and producing colored traces (tautomeric reaction of the dye) by irradiation with a narrow beam of ultraviolet light from a giant pulse ruby laser with frequency doubler. Quantitative measurements were made from high speed movies.

Prior to the present study, only qualitative fluid flow measurements using suspended metal powder have been obtained in the system. Theoretical studies with many assumptions have been made by Macagno and Hung (1966) and Le Feuvre (1969).

CONCLUSIONS AND SIGNIFICANCE

A nondisturbing flow visualization technique has been used to study the flow properties of a laminar pipe jet with flat entering velocity profile. The Reynolds number range from 90 to 1,355 based on the nozzle diameters was investigated.

1. Mean axial and radial velocities at different distances from the jet entrance were measured and calculated as a function of radial position y/D_N for the range of Re studied.

2. The present experiments have shown the existence of regular waves in the region of the detached shear layer that bounds the jet emerging from the circular orifice of the nozzle. The existence of these periodic fluctuations helps explain previous large differences between theoretically predicted and measured mass transfer coefficient.

Furthermore, as the attachment is approached, the flow becomes increasingly irregular or "turbulent." Approaching the re-attachment zone, the flow acquires, in addition to the motion along the tube axis and the radial motion, a substantial circumferential component. The effects of these phenomena have not been included in the theoretical predictions. These wavelike instabilities were observed

Correspondence concerning this paper should be directed to J. W. Smith. F. Frantisak is with International Nickel Co. Ltd., Toronto, Canada.

throughout the whole Reynolds number investigated.

3. A clear transition in the waves from irregular sinusoidal to varicose was observed at $Re_N = 350$. Above this Reynolds number, the position of the re-attachment zone fluctuated widely. The varicose wave behavior was not observed in a pipe jet with developed laminar starting profile at $Re_N = 754$.

4. The frequencies of the waves, expressed as Strouhal numbers, agree reasonably well with those reported by Becker and Massaro (1968) for a free jet with flat velocity profile. The displacement between the two curves is attributed to the effect of the pipe wall on the oscillation. The shedding frequency is a direct function of the square root of Reynolds number. In the same graph the experimental data of Beavers and Wilson (1970) for a parabolic entering profile jet in a water tunnel are also plotted. These authors found the Strouhal numbers for Reynolds larger than 700 and approximately the same entrance orifice diameter as ours to be independent of the flow rate and equal to 0.63.

5. The position of the re-attachment zone was found to move downstream with increasing Re until the transition at $Re = 350$, above which it approached the limiting value of $\frac{x}{D_N}$ of about 3 obtained from Runchal's work (1969).

6. Instantaneous wall shear stresses calculated from the velocity gradients agreed qualitatively with the theoretical prediction of Le Feuvre (1969), which does not account for wave behavior.

7. After the re-attachment zone, the recovery of flow from the effect of separation is gradual. At $\frac{x}{D_N} = 15.5$ the velocity profile was still only partially developed.

The series of experiments reported in this paper were designed to provide information and a better understanding of the behavior of a laminar incompressible flow behind a sudden enlargement of a pipe.

For an optimum design of an engineering device, the location of the re-attachment zone is very important. The heat and mass transfer coefficients here are three of four times greater than in the region further downstream, where regular pipe flow becomes re-established.

An understanding of mass and heat transfer phenomena in separated flow regions such as occur in the pipe jet cannot be reached unless fluid flow characteristics are known. These have been obtained quantitatively and reliably for the first time in a sudden pipe expansion and are reported in this paper.

Separated flows are often encountered in engineering problems and result in advantages, such as an increase in transfer rate, or disadvantages, such as an increase in the pressure loss. Because of the experimental difficulties involved, relatively few experimental measurements have been made in this field.

If the diameter of a pipe suddenly expands, the flow separates from the wall and re-attaches again in a region downstream; such a situation is sometimes called a pipe jet. Two entering velocity profiles are of general interest: the flat profile and the Poiseuille profile. A nearly flat profile was obtained in this work using a specially-designed nozzle.

Figure 1b illustrates the circular pipe with a sudden expansion in which the steady flow pattern may be considered as composed of a main stream gradually increasing in diameter from the edge of the expansion to the re-attachment point and an annular eddy enclosed between the surface of the main stream and the walls of the tube. Hence there is a central region with a positive velocity in the x direction, surrounded by a shell of liquid moving in the opposite direction. The central positive region expands with increasing distance x from the expansion until it reaches the wall at the zone of attachment. A surface of zero axial velocity passes through the center of the eddy and separates the positive core from the negative shell. Flow in the negative shell could be considered approximately annular, but with a flow of liquid radially through the surface of zero axial velocity.

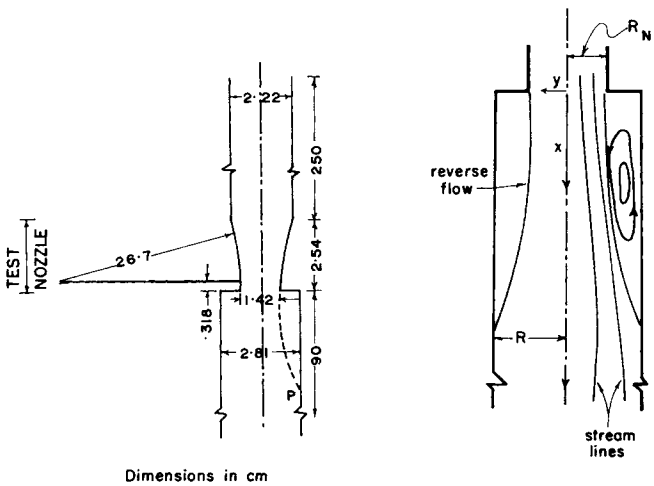

Fig. 1. The pipe jet—a sudden enlargement in a circular pipe a. test nozzle, b. the geometry of the pipe jet.

The separation that occurs at the edge of the expansion step produces a free shear layer between the main stream and the annular eddy.

Thom (1932) first studied analytically the difficult hydrodynamic problem in a pipe jet and obtained a numerical solution at a Reynolds number of 10.

Macagno and Hung (1966) produced a computer simulation of the laminar flow and experimentally visualized the flow by suspending aluminum powder in a test mineral oil and recording the stream lines photographically. More recently Spalding (1969) presented a numerical finite-difference procedure for the solution of the full, elliptic, partial-differential equations of steady two-dimensional flows with recirculation. LeFeuvre (1969) applied the procedure to predict the laminar flow downstream of a sudden enlargement in a circular pipe, and Runchal (1969) studied the turbulent problem. Experimental studies have been confined mainly to heat transfer and turbulent flow. Ede and co-workers (1956, 1962) reported local heat transfer coefficients and the results of flow visualization experiments for water flowing through a pipe jet with an expansion divergence ratio of 1:2. Seban et al. (1959) measured local heat transfer coefficients downstream of a surface step for the flow of air. Krall and Sparrow (1966) also determined local heat transfer coefficients for fluids with Prandtl num-

bers between 3 and 6 for the same geometry. Mass transfer measurements have been made recently by Runchal (1969, 1971) for very high Schmidt numbers in turbulent flow.

The results of all these workers may be summarized as follows: heat or mass transfer coefficients are less than in steady developed pipe flow immediately after the separation; further downstream in the re-attachment zone than in the pipe these coefficients become as much as two or three times higher.

Hummel's flow visualization technique permits the completely nondisturbing study of complex flows and on Spalding's suggestion was applied to the study of flow in the pipe jet.

The photochromic technique is nondisturbing because a beam of ultraviolet light is used to introduce a colored dye trace in a solution containing a photochromic dye. The trace can then be followed with a high speed motion picture camera. Quantitative measurements with as good time and space resolution as are obtainable from hot wire anemometry techniques are attainable with the technique.

Properties of the flow investigated in these experiments include the steady behavior before the re-attachment zone and near the jet entrance, the periodic behavior of the waves, the apparently random behavior near the re-attachment point, and the region after the attachment point.

EXPERIMENT

Test Solutions Used

The test solutions were prepared using two different dye materials: 2-(2′,4′-dinitrobenzyl)pyridine (DNBP) dissolved in ethyl alcohol and the spiropyran: [TMINBPS: E. Fisher private communication; Koelsch and Workman (1952)] dissolved in kerosene. The physical properties of these solutions are tabulated in Table 1, together with other experimental conditions.

Both indicators respond with maximum optical density in the UV region (Hardwick et al., 1960; Berman et al., 1959).

The first indicator dye, DNBP was used in work described elsewhere (Popovich and Hummel 1967; Frantisak et al., 1969). The TMINBPS indicator material produces an excellent blue trace in kerosene which when photographed with a yellow sodium lamp gave good contrast, and it has been used for most of the experiments described here.

The nitrospyran reaction is

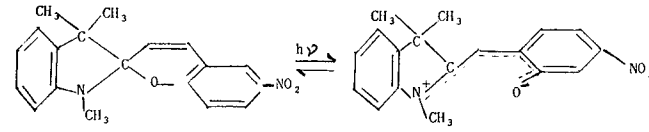

From the above equation, it can be seen that the color is produced as a result of breaking of the carbon-oxygen bond in the spiropyran ring, producing a merocyanine structure. This reaction is reversible spontaneously after a few seconds so that one may work under normal illumination without an accumulation of color. The time stability of the dye, however, is long enough for all the measurements required.

The indicator solutions tend to decompose on long standing, and freshly prepared solutions were used for these experiments. The low concentration of solid dye added to the solvent (0.1% by weight in the case of DNBP and 0.02% by weight in the case of TMINBPS) were not sufficient to affect the density and viscosity of the solvent.

Optical Arrangement

Figure 2a is a schematic diagram of the apparatus. A giant pulse ruby model TRG-104A laser with a peak power up to 100 MW and a wavelength 6943Å was used. A second harmonic generator reduced the wavelength to ½, and at the same time reduced the energy. Taking into account the additional losses due to the optical systems, the energy of the resulting trace may be estimated to be roughly 0.01 joule or less. The pulse had a duration of about 30 nanoseconds and the trace was formed in less than three microseconds (Mosher et al., 1962). Under certain conditions, the diameter of the beam has been reduced to about 25μ.

The laser beam (Figure 2a and c) was directed normally to one of the test section walls in order to avoid refraction. The lenses contracted the beam with the focus of the second lens falling into the liquid. The camera was placed at 90° to the beam path and the light source (sodium lamp) located behind the test section on the optical axis of the camera. The opening of the camera was synchronized with the triggering of the laser power supply.

A better qualitative visualization of the flow can be obtained by using a continuous source of UV light, rather than the laser, which can only be triggered infrequently because of the time required to accumulate electrical charge in the power supply and to cool the ruby. In this work, the Phillips CS-100 watt mercury lamp was placed in the position normally occupied by the laser head, as illustrated in Figure 2b, or nearly parallel to the movie camera at 90° to the laser beam Figure 2c. The optical system included two rectangular mirrors and lenses

Table 1. Experimental Conditions and Data

Input energy to the laser 750 Joules

Indicator conc., wt. %	Solvent conc., wt. %	Solution temp., °C.	$\nu \times 10^2$ cm²/s	Re	Re_N	f cps	S	Reattachment zone, x cm	x/D_N
0.10 DNBP	ethylalcohol 95% ($\rho = 0.800$)	22	1.69	581	1166	—	—	6.81-9.93	4.80-7.00
				666	1355	9.80	0.560	5.60-9.76	3.95-6.88
				540	1100	8.10	0.565	6.66-10.5	4.70-7.40
				389	754	7.83	0.442	7.70-11.9	5.43-8.40
				253	503	—	—	15.6-17.2	11.0-12.1
				213	422	—	—	17.3-19.8	12.15-13.9
0.02	Kerosene			149.5	296	—	—	18.2-19.2	12.8-13.5
Nitrospyran	($\rho = 0.805$)	25	2.75	104	205	—	—	12.5-13.0	8.8-9.16
				76.2	151	—	—	9.0-10.0	6.3-7.05
				63.7	125	—	—	6.6-6.8	4.65-4.78
				58.2	118	0.246	0.159	—	—
				46.5	92	—	—	5.8-6.0	4.07-4.20
				43.2	88.5	0.236	0.203	—	—

which produced five beams of UV light. A shutter was used to interrupt the beam of light at different time intervals. Heat effects produced by the lamp were minimized by locating it at a distance of about 70 cm from the test section and by using long focal length quartz lenses. At low flow rate or in regions of low flow rate, great care was taken to insure that no local heating or cooling effects affected the flow.

Other experimental details, such as optical and photographic materials, have been described previously by Frantisak et al. (1969) and Iribarne et al. (1969).

Apparatus: The Flow Circuit and Test Section

A schematic diagram of the apparatus used is given in Figure 3. Vibrations were avoided by using only the hydrostatic head of the liquid in a vertical system to obtain the flow. Fluid flowed from tank 1 through a nest of 1 mm diameter by 10 cm long glass capillaries to insure uniformity of the stream lines and to dampen any vibrations resulting from the flow from the upper tank. The nozzle and expansion section illustrated in Figure 1a was situated 250 cm or 180 diam. downstream from the flow straightening section. The total length of the vertical section was 345 cm. The nozzle used was designed by Dr. Runchal of the Imperial College to provide a flat velocity profile and to reduce the thickness of the boundary layer to a minimum. All experiments were conducted downstream of the sudden expansion to and below the re-attachment zone (Point P, Fig. 1a). The axes of the small and large tubes were made to coincide exactly by visual observation of the jet.

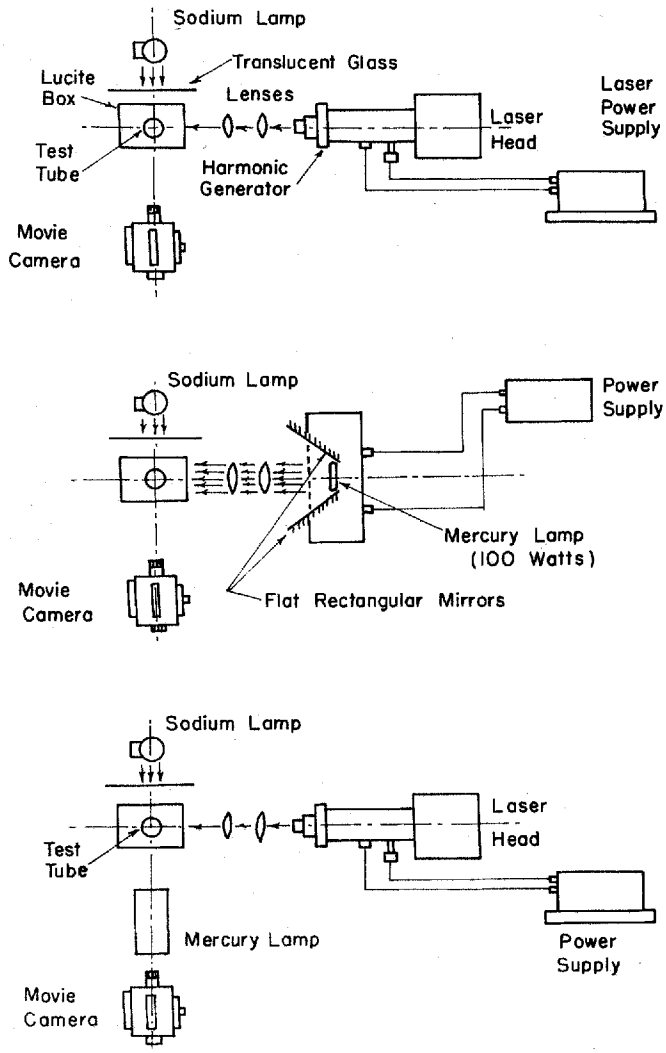

Fig. 2. Optical arrangements of the test equipment. a. The laser beam normal to the test section and camera axis. b. UV beam from the mercury lamp normal to the test section. c. As in (a) but with the mercury lamp parallel to the camera.

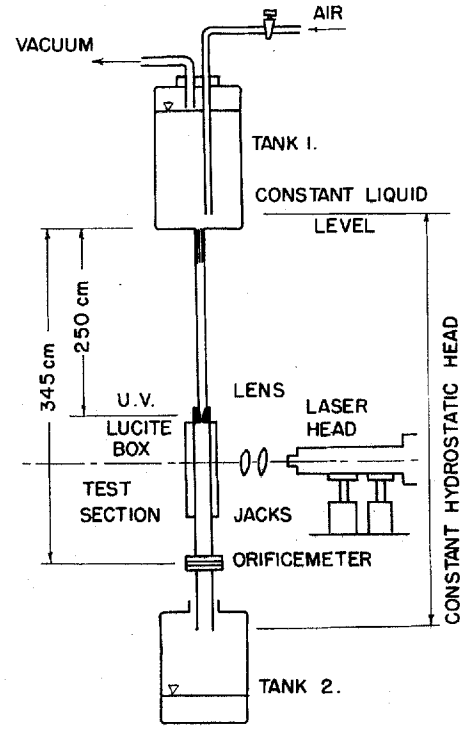

Fig. 3. Schematic diagram of the flow system.

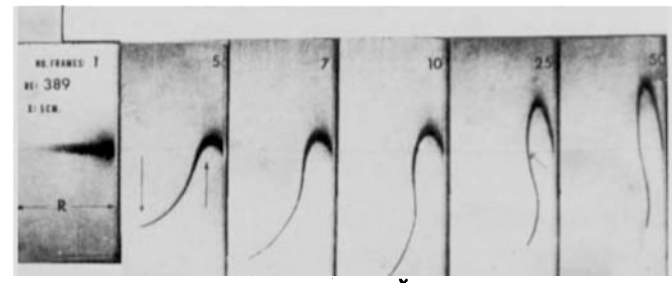

Fig. 4. A sequence for $Re = 389$ and $\frac{x}{D_N} = 0.56$. Frame numbers are shown in the figures. Time per frame = 0.01656 sec.

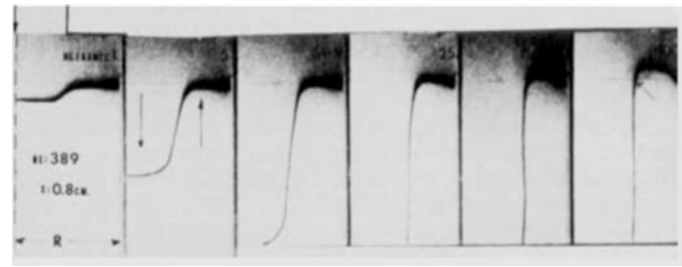

Fig. 5. A sequence of frames for $Re = 389$ and $\frac{x}{D_N} = 3.53$. Time per frame = 0.01656 sec.

A square plexiglass box filled with the test liquid was installed to reduce optical distortion caused by the round tube.

The laser head was mounted on two jacks which permitted vertical alignment.

INTERPRETATION OF EXPERIMENTAL DATA

Typical experimental results are shown in Figures 4 and 5, which are two sets of sequences of pictures of the trace at different times for $Re = 389$ and $x = 0.8$ cm and 5.0 cm respectively. These figures illustrate clearly the regions of the main and reverse flow. The points corresponding to

zero axial velocity are shown with an arrow in two of the pictures.

Frame 100 in Figure 4 gives the position of the dye trace 1.5 seconds after the triggering of the laser. The distance travelled by the trace is proportional to the velocity of flow in a particular region. Thus, the velocity in the region of reverse flow is much greater 5 cm downstream, as shown in Figure 5 than 0.8 cm downstream as shown in Figure 4. The distance travelled by the peak of the distorted parabola after 50 frames, the same time interval, is much greater in Figure 5 than in Figure 4. It is also apparent that the thickness of the annular region is changing with distance from the expansion region.

The instantaneous axial velocity $u(y, t)$ of the trace can be determined from the change position of the traces

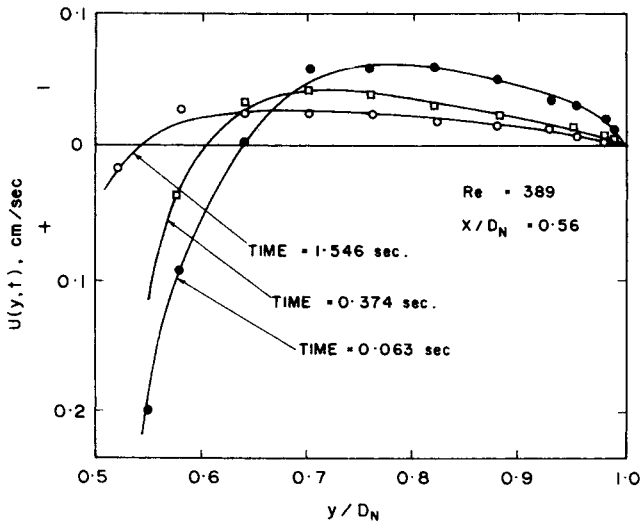

Fig. 6. Time variation of the velocity profile. $Re = 389$; $x = 0.8$ cm.

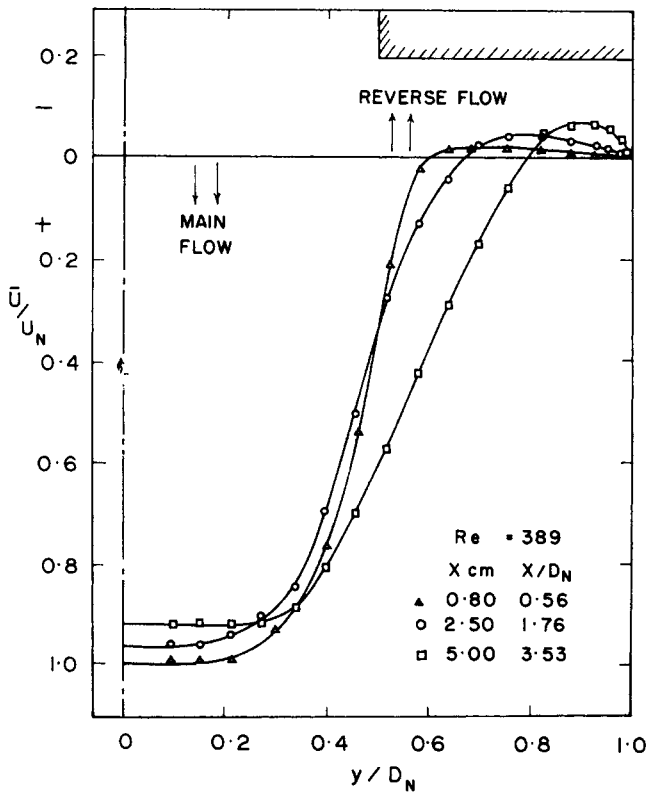

Fig. 7. Velocity profiles at different distances x from the jet entrances. $\mu_N = 16.9$ cm/sec; $Re = 389$.

frame-by-frame and the time between frames. For reasons discussed below, the accuracy with which $u(y, t)$ can be calculated for a given x depends on the framing rate.

Typical trace velocities for the nominal axial position $x = 0.8$ cm ($x/D_N = 0.56$) and for $Re = 389$ are shown in Figure 6. The instantaneous trace velocities are plotted as a function of y/D_N, where y is the distance from the center of the tube normal to the wall and D_N is the diameter of the nozzle. Because the trace is moving upstream in the region of annular flow and downstream in the core region, its velocity distribution changes with time since the axial position of each fluid element changes with time and the velocity distribution depends on axial position x. The distances between traces divided by the time increment give average axial velocities for the time increment and for the space traversed by the dye trace. These calculations are strictly valid only if the flow is unidimensional. However, radial velocities were calculated by mass balance, and as discussed later, no corrections were made. With the sufficiently small time increments used here, no correction was required for the change in velocity of the trace with axial position.

The value of u_N, the axial velocity in the center of the jet at the nozzle, was determined by measurement because the velocity profile is not completely flat at the nozzle exit. The centerline value of the velocity in the jet was determined for different axial positions and the value at the nozzle was then determined by extrapolation. u_N was about 5% greater than u_{av}, the average velocity in the nozzle.

In general, the data given in this investigation are the average of at least 10 traces obtained under the same conditions. In steady flow the standard deviations of the means were up to 3.5% of the velocity values.

RESULTS

Behavior Near the Jet Entrance

At various axial locations near the jet entrance, averaged axial velocity profiles like those shown in Figure 7 were obtained for $Re = 389$. The spread of the jet is apparent, as is the development of the flow reversal near the wall. These velocity profiles were very reproducible and bore little resemblance to those obtained near the re-attachment point. Little or no evidence of the wave formation and patterns which are characteristic of the flow near the re-attachment point was observed in the region close to the jet entrance. Figure 7 is a dimensionless plot of u/u_N at different distances x from the jet entrance. Negative values of the velocity ratio, therefore, represent regions of flow reversal.

Figure 8 is a plot of the distribution of the mean velocity relatively close to the wall region. A velocity profile obtained far downstream from the nozzle entrance at $x = 22$ cm is shown on the figure as a dashed line. Also plotted on the graph is a line which represents the laminar velocity profile for $x/D_N \rightarrow \infty$ (that is, fully developed flow).

The radial velocity component $\bar{V}$ in the y direction, where y is the distance from the center line, can be readily calculated from a mass balance and the axial velocities if the flow is two-dimensional and steady. The results plotted in Figure 9 as dimensionless velocity $\bar{V}/u_N$ against dimensionless radial position y/D_N show that except very near the nozzle and in the annular zone radial velocities are much less than axial velocities at the same axial position. The inflections at 0.40 and 2.50 cm occur at a y/D_N of approximately 0.5 immediately below the nozzle and in the region of maximum shear. Since the change is from

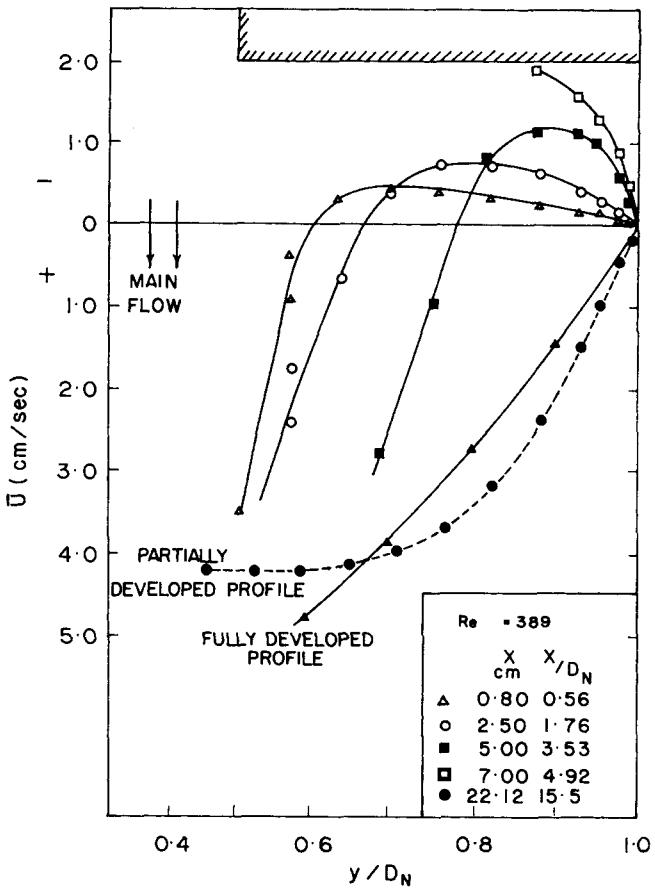

Fig. 8. Velocity profiles before and after the re-attachment zone $Re = 389$.

positive to negative, the direction of radial flow changes suddenly from away from the center to towards the center. Further downstream, the results show the expected flow of fluid from the core to the wall region as the annulus shrinks.

No correction to the axial velocities was made although in principle one is necessary because the radial velocities were generally much less than the axial velocities.

Formation of Waves

The flow separation that occurs at the edge of the nozzle produces a laminar free shear layer, which lies between the internal stream and the region of low velocity in annular flow. The existence of fluctuations in this region is an important finding in the present work. These disturbances are regular pulsations or oscillations in the detached shear layer. They were postulated by Charwat et al. (1961), to account for an unsteady flow in an airflow passing over a notch (cavity) found using a spark Schlieren photography method. Reiman and Sabersky (1968) also noticed regular oscillations in the free shear layer of laminar flow over a set of transverse rectangular slots.

More recently, Becker and Massaro (1968) studied the stability of an axisymmetrical jet with a flat velocity profile. The air stream was made visible with a mist of condensed oil. The jet was subjected to different acoustic excitations, but measurements were also made of the shedding frequencies with minimal laboratory noise (in "silence").

Other recent studies in this field include the work of Beavers and Wilson (1970). It contains observations on a regular periodic flow at a bounding jet emerging from a sharp-edged two dimensional slit or a sharp-edged circular orifice. The experiments were carried out in a water rectangular tunnel for Re 500-3000. Visualization of the flow field was realized by introduction of dye through small tubes. These and Becker's and the present results are compared in this paper.

The instabilities are best illustrated by traces generated with the continuous UV light source. The laminar boundary layer remains laminar for some considerable distance after it leaves the nozzle before fluctuations begin. For very low velocities, as shown in Figure 10, the fluctuations are sinusoidal. Only one half of the jet is shown, because the trace did not penetrate the entire jet.

The crest of the wave has been indicated with an arrow on both photographs, the right-hand one corresponding to some time later than the left-hand one. When the mean velocity increases, the instability becomes varicose at a $Re_N \geqq 350$ and the waves roll down into a succession of ring vortices as shown in Figure 11. The instability is attributed to the sharp change in velocity between the jet and relatively stagnant annular eddy. The varicose behavior was not observed in a pipe jet with a developed laminar starting profile at $Re_N = 754$.

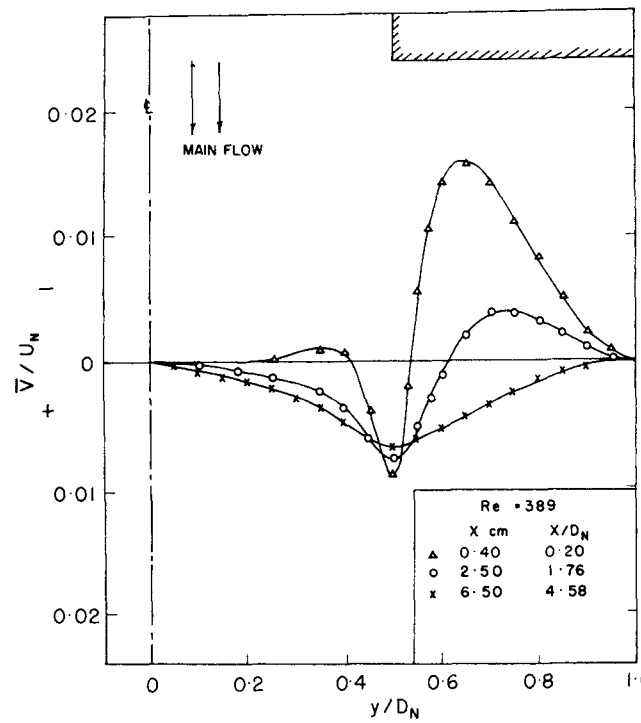

Fig. 9. Radial velocity at different distances x from the jet entrance $Re = 389$.

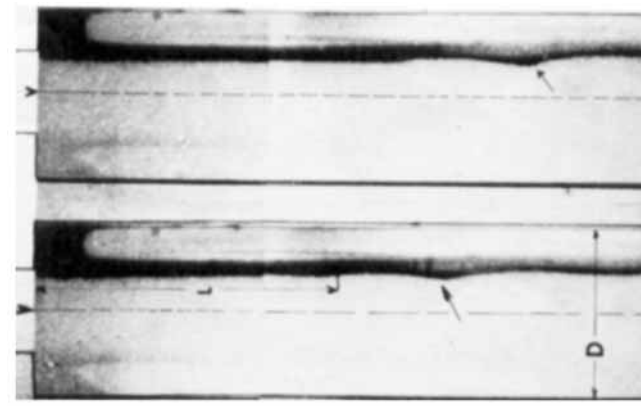

Fig. 10. Sinusoidal fluctuations, $Re = 58.2$. The arrows indicate the crest of the waves.

Analysis of the waves show that they are not completely regular, and their amplitudes and tendency to crest changes periodically. These differences are, in part at least due to the tangential movement. It was observed that the vortices disintegrate as they come close to the re-attachment zone.

The frequency of the waves was determined using two techniques: stroboscopic illumination and direct reading on the films. Direct reading required the analysis of a great number of frames.

The distance L from the nozzle mouth to the point at which the waves fold or roll back, also called the 'wave-breaking length', was found to be a function of the square root of the reciprocal of the Reynolds number. The length L can be easily observed in Figures 10 and 11.

The shedding frequency is usually expressed in terms of the dimensionless Strouhal number ($f\ D_N/u_N$) against the Reynolds number based on the nozzle diameter as shown in Figure 12. The curve of Becker and Massaro (1968) for free-jet vortex shedding frequency in "silence" has also been plotted for comparison. The slopes are the same (0.5), but there is a displacement which may be attributed to the effect of the pipe wall on the oscillation. These results indicate that the shedding frequency S is a direct function of the square root of the Reynolds number

$$S = \text{constant}\ Re_N^{1/2}$$

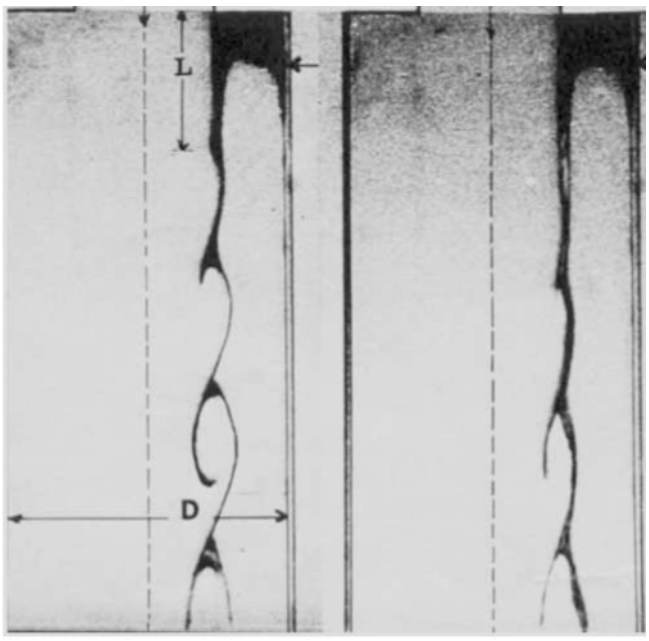

Fig. 11. Varicose fluctuations, $Re = 389$.

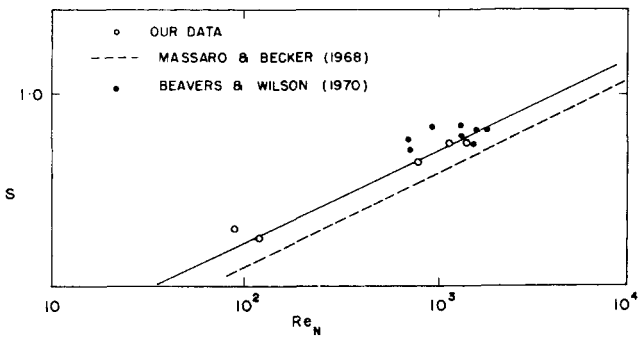

Fig. 12. Strouhal number versus nozzle Reynolds number.

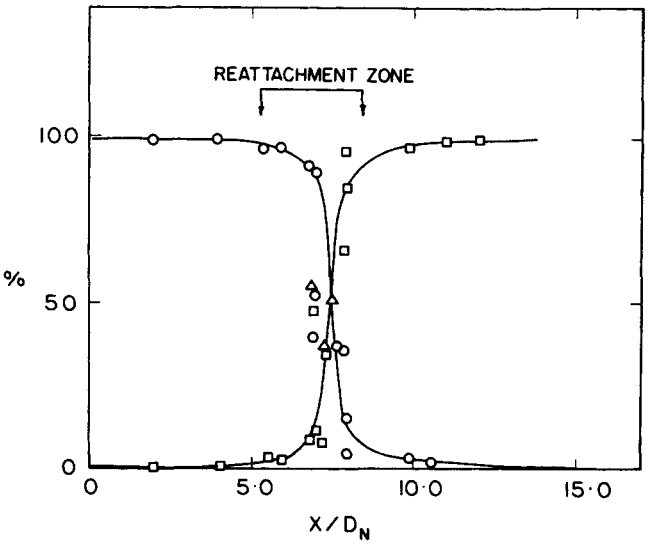

Fig. 13. Frequency distribution of up and downward motion at the wall as a function of $\frac{x}{D_N}$, $Re = 389$; 0 = up; + = down; Δ = up and down in the same frame.

The black points on the same graph represent the measurements obtained by Beavers and Wilson (1970). They found that the Strouhal numbers for both the plane and axisymmetric jets are independent of the Re numbers.

The Re-attachment Zone

Because of the waves, the flow in the re-attachment zone is very irregular, and the position of the re-attachment point oscillates up and down stream around a mean value of x for a given Reynolds number. The dye traces were observed in the motion pictures to flow sometimes upwards and sometimes downwards, and tended to swirl around the wall at a velocity which was frequently large relative to the velocity in the axial direction. This unsteady condition led to considerable experimental difficulty in determining the re-attachment region. The laser and mercury lamp were used in different positions as described in Figures 2b and 2c to explore the re-attachment region. It was generally easier to determine the length of the eddy or distance to the re-attachment point at very low Reynolds numbers, because then the fluctuations are sinusoidal and the propagation velocity of the waves is very low (0.156 cm/s for $Re_N = 118$). For these very low Reynolds numbers, the re-attachment can be said to occur at a definite point rather than in a zone. (See Table 1.)

Higher stream velocities required the analysis of about 7,000 frames (about 10 min. of film) for each re-attachment distance and the criterion adopted for its determination at a given value of Re was as follows: In the upper region near the nozzle every trace shows an upward motion near the wall. Downstream, at a sufficiently great distance from the jet entrance, the opposite is true. Along an intermediate interval of the distance x, successive traces will show both upward and downward motion. This region has been called the re-attachment zone. In this interval the frequency of upward motion as shown by different traces varies continuously from 100 to 0%, defining the upper and lower limits of that zone. Frequency distribution curves were computed and plotted for upward and downward motions, an example of which is given in Figure 13 for $Re = 389$. Here the re-attachment zone is found to lie approximately between 5 and 8 for the values of x/D_N, hence the interval is about 4 cm. The triangles in this graph indicate observations in the middle region where

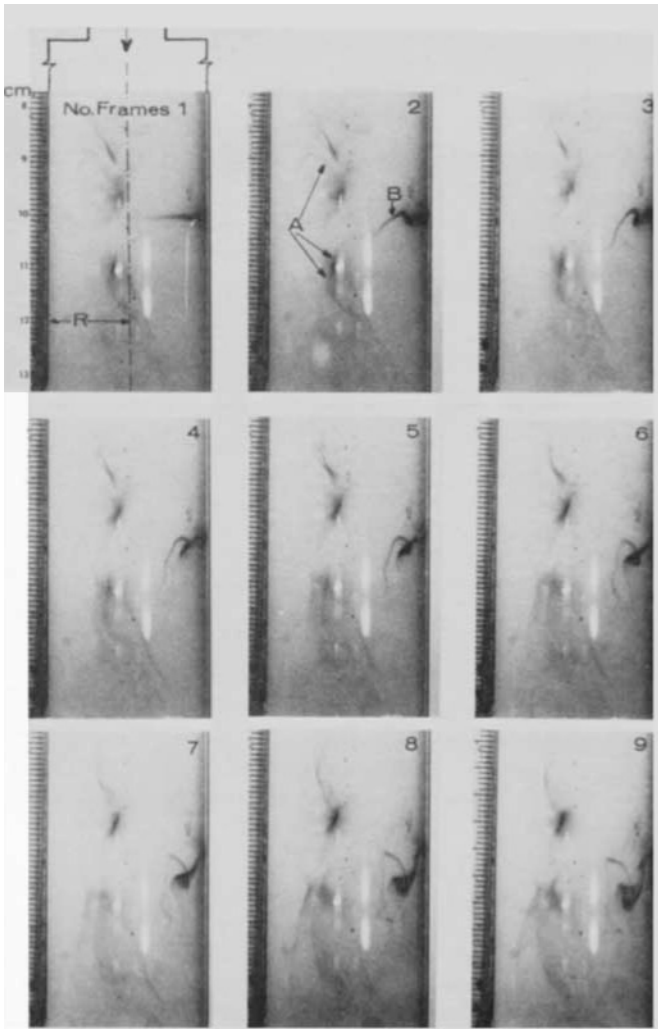

Fig. 14. Sequence of frames for $Re = 389$ at the re-attachment zone using the optical arrangement of Figure 2c (time per frame = 0.0413 sec).

changes in the direction of motion occurred so quickly that different traces in the same frame, 1/12 sec., moved in different directions.

Figure 14 illustrates for $Re = 389$ fluctuations in the vicinity of the attachment point. Both the mercury lamp and the laser were used in this figure. The mercury lamp beams (lines A on the picture) penetrate into the liquid parallel to the camera at 90° from the laser beam (line B).

The concentration of the indicator was doubled to reduce the penetration length of the trace which also increases its intensity for better observation of the tangential and axial turbulence near the wall. In these frames it is possible to observe the chaotic motion of the traces in the x and y direction and around the wall in a circumferential movement. Shortly after the trace had been introduced with the laser at the right wall it became irregular bending while moving from one side to the other in the liquid. Practically no trace in the re-attachment frame was like another, indicating a high degree of turbulence in this region. This turbulence undoubted is responsible for much of the increase in heat and mass transfer in this region.

Figure 15 shows the lengths of the separated regions expressed as x/D_N, against Re based on the nozzle diameter and are also included in Table 1.

The vertical segments indicate the re-attachment zones with their upper and lower limits computed as illustrated in Figure 13.

The data of Macagno and Hung (1966) for an entering parabolic profile and Reynolds number up to 200 are plotted on the same graph. They are in quantitative agreement with our results over the same range of Reynolds number.

Also shown on the graph are the theoretical predictions of LeFeuvre (1969) shown as a dashed line. This prediction was made for a completely flat entering velocity profile, and momentum transfer due to the formation of waves was not taken into account in their model.

For higher Reynolds number (> 5,000) Runchal's (1969) measurements obtained using an electrochemical method, are also represented for Schmidt numbers 1,400 and 2,500. The points indicate the locations where the mass transfer coefficients were found to be a maximum, which are expected to correspond with the location of the re-attachment zone.

On this figure, it can be seen that the re-attachment point moves farther from the nozzle as the Reynolds number is increased up to approximately 350, and then begins to fall again.

A change in the flow regime at a Re_N of 350 is clearly indicated by this change. A considerable tangential motion was observed at this Re, but not at the lower Re (90) studied. Development of the tangential motion is therefore most likely responsible for the change in the behavior of the re-attachment zone.

Below a Re_N of 350, the re-attachment zone, as defined earlier and illustrated in Figure 13, is very small. Above $Re_N = 350$, the observed zone was much longer.

As the stream velocity increases, the attachment zone moves closer to the nozzle, apparently approaching a constant position, as indicated by the results obtained from the mass transfer data.

After the re-attachment of the boundary layer, the flow returns gradually to a parabolic velocity profile. Although flow reversal is no longer present, the measurements indicated that in this region the flow is still under the influence of the pipe jet. As an example, Figure 16 for $x = 13$ cm and $Re = 389$ shows the influence on the trace of large eddies. At about 22 cm downstream (Figure 8) the velocity profile was found to be only partially developed.

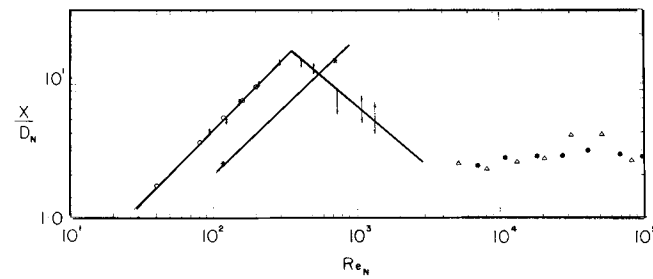

Fig. 15. Variations of relative eddy length versus nozzle Reynolds number. Dashed line: predictions of LeFeuvre (1969), ○ Macagno and Hung (1967), ⇕ Present work, and △ Runchal (1969) $Sc = 2500$ ● $Sc = 1400$.

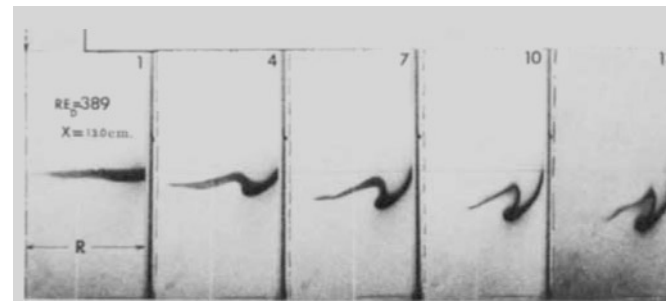

Fig. 16. Sequence of frames for $Re = 389$ after the re-attachment zone at $x = 13.0$ cm (time per frame = 0.0413 sec).

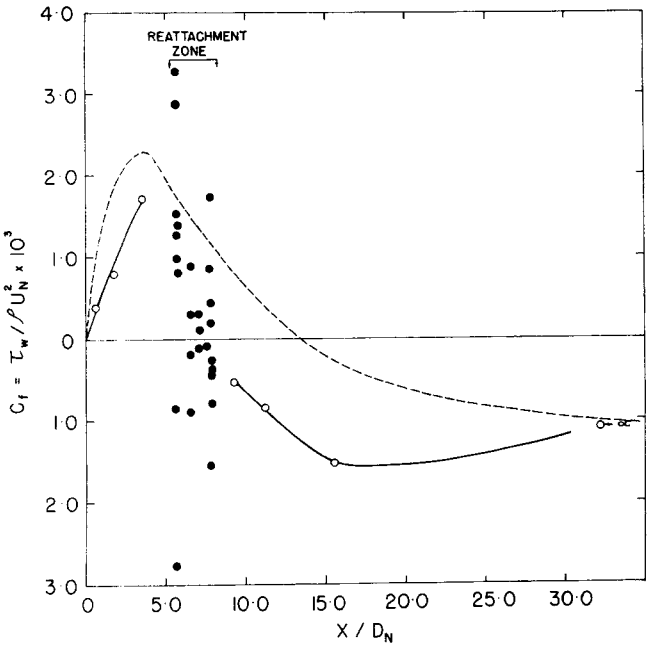

Fig. 17. Nondimensional wall shear stress versus X/D_N for Re = 389. Dashed line: predictions of LeFeuvre (1969) ○ time-average values ● instantaneous values present work.

Wall Shear Stresses

The instantaneous values of the wall shear stress were calculated from the velocity gradient in the viscous sublayer $\tau_w = \mu \left(\frac{du}{dy}\right)_w$ where μ is the dynamic viscosity. The instantaneous wall shear was calculated from successive picture frames and the overall average value $\overline{\tau}_w$ was computed for each trace sequence. The nondimensional wall shear stress expressed as $C_f = \overline{\tau}_w/\rho\ u_N{}^2$ is plotted against x/D_N for Re = 389 in Figure 17. For the region of re-attachment, some instantaneous values, shown as black points, of this nondimensional group are also shown on the graph. They illustrate the chaotic movement upwards and downwards of the flow in this region. The point on the right represents the calculated shear-stress for fully-developed flow. On the same graph, the theoretical curve obtained by LeFeuvre, is plotted as a dashed line. LeFeuvre's analysis did not include the effect of instabilities (sinusoidal or varicose) and hence would not be expected to predict the experimentally measured values. Agreement is qualitative, however.

ACKNOWLEDGMENTS

We are indebted to Professor D. B. Spalding for suggesting this work and for his invaluable advice. Helpful discussions with Dr. D. A. Gosman, Dr. A. Runchal, and Mr. LeFeuvre from Imperial College are also appreciated. Financial assistance from the Ford Foundation and the National Research Council of Canada is gratefully acknowledged.

NOTATION

C_f = nondimensional wall shear stress $(\overline{\tau}_w/\rho\ u_N{}^2)$
D = big diameter pipe = 2.81 cm
D_N = diameter nozzle = 1.42 cm
DNBP = 2-(2′,4′-dinitrobenzyl)pyridine
f = wave frequency
L = distance from the nozzle mouth to the point where the waves fold or roll back
R = radius big pipe
R_N = radius nozzle
Re = Reynolds number based on big diameter pipe
Re_N = Reynolds number based on nozzle diameter
S = Strouhal number $(\equiv f \cdot D_N/u_N)$
TMINBPS = 1,3,3-trimethyl-6′-nitroindoline-2-spiro-2′-benzopyran
$\overline{U}$ = mean velocity in x direction
u_{av} = average velocity at the nozzle
U_N = velocity at the center of the nozzle
$U(y, t)$ = instantaneous velocity in x direction
$\overline{V}$ = mean velocity in y direction
x = axial distance measured from the sudden enlargement (x = 0 at the jet entrance)
y = distance from the center, normal to the wall
w = evaluated at the wall

Greek Letters

μ = dynamic viscosity
ν = kinematic viscosity
ρ = density
τ_w = instantaneous value of wall shear stress
$\overline{\tau}_w$ = average value shear stress

LITERATURE CITED

Beavers, G. S., and T. A. Wilson, "Vortex growth in jets," *J. Fluid Mech.*, **44**, 97 (1970).

Becker, H. A., and T. A. Massaro, "Vortex evolution in a round jet," *ibid.*, **31**, 3, 435 (1968).

Berman, E., R. E. Fox, and F. D. Thomson, "Photochromic Spiropyrans," *J. Am. Chem. Soc.*, **81**, 5605 (1959).

Charwat, A. F., J. N. Roos, F. C. Dewey, and J. A. Hiltz, "An investigation of separated flows. Part I: The pressure field. Part II: Flow in the cavity and heat transfer," *J. Aerospace Sci.*, **28**, 457; *ibid.*, 513 (1961).

Ede, A. J., C. I. Hislop, and R. Morris, "Effect on the local heat-transfer coefficient in a pipe of an abrupt disturbance of the fluid flow: abrupt convergence and divergence of diameter ratio 2/1," *Proc. Inst. Mech. Eng.*, **170**, 38 (1956).

Ede, A. J., R. Morris, and E. S. Birch, "The effect of abrupt changes of diameter on heat transfer in pipes," NEL Rept. 73, National Eng. Lab., East Kilbride, Glasgow, Scotland (1962).

Fischer, E., The Weizmann Institute of Science, Rehovoth, Israel, private communication (1965).

Frantisak, F., A. Iribarne, J. W. Smith, and R. L. Hummel, "Nondisturbing tracer technique for quantitative measurements in turbulent flow," *Ind. Eng. Chem. Fundamentals*, **8**, 160 (1969).

Gosman, A. D., W. M. Pun, A. K. Runchal, D. B. Spalding, and M. Wolfshtein, "Heat and mass transfer in recirculating flows," Academic Press, London and New York (1969).

LeFeuvre, R., Mech. Eng. Dept., Imperial College, London, private communication (1969).

Hardwick, R., H. S. Mosher, and P. Passailaique, "Photochromotropic behaviour of 2-(2′, 4′-dinitrobenzyl)-pyridine," *Trans. Faraday Soc.*, **56**, 44 (1960).

Iribarne, A., F. Frantisak, R. L. Hummel, and J. W. Smith, "Transition and turbulent flow parameters in a smooth pipe by direct flow visualization," *Chem. Eng. Progr., Symp. Ser., No. 91*, **65**, 60 (1969).

Koelsch, C. F., and W. R. Workman, "Some thermochromic spirans," *J. Am. Chem. Soc.*, **74**, 6288 (1952).

Krall, K. M., and E. M. Sparrow, "Turbulent heat transfer in the separated, reattached and redevelopment regimes of a circular tube," ASME, *J. Heat Transfer*, **88**, 1, 131 (1966).

Macagno, E. O., and T. K. Hung, "Computational and experimental study of a captive annular eddy," *J. Fluid Mech.*, **28**, 1, 43 (1966).

Mosher, S. H., E. R. Hardwick, and D. Ben Hur, "Flash-photolysis studies of α- and γ-(2, 4-dinitrobenzyl)pyridine," *J. Chem. Phys.*, **37**, 4, 904 (1962).

Popovich, A. T., and R. L. Hummel, "A new method for nondisturbing turbulent flow measurements very close to a wall," *Chem. Eng. Sci.*, **22**, 21 (1967).

Reiman, T. C., and R. H. Sabersky, "Laminar flow over rectangular cavities," *Intern. J. Heat Mass Transfer*, **11**, 1083 (1968).

Runchal, A. R., "Transfer processes in steady two-dimensional separated flows," Ph.D. thesis, Imperial College, London, England (1969).

Runchal, A. R., "Mass transfer investigation in turbulent flow downstream of sudden enlargement of a circular pipe for high Schmidt numbers," *Intern. J. Heat Mass Transfer*, **14**, 781 (1971).

Seban, R. A., A. Emery, and A. Levy, "Heat transfer to separated and reattached subsonic turbulent flows obtained downstream of a surface step," *J. Aerospace Sci.*, **26**, 809 (1959).

Spalding, D. B., "The prediction of two-dimensional, steady, turbulent elliptic flow," Intern. Seminar Heat Mass Transfer in Flows with Separated Regions and Measurements Techniques," Herceg-Novi, Yugoslavia (1969).

Thom, A., "Arithmetical solution of problems in steady viscous flow," Aeron. Research Com. Rpts. Memoranda No. 1475, London (1932).

Manuscript received October 26, 1971; revision received February 4, 1972; paper accepted February 11, 1972.

The Kinetics of Alkylation of Isobutane with Propylene

J. RANDOLPH LANGLEY and RALPH W. PIKE

Department of Chemical Engineering
Louisiana State University, Baton Rouge, Louisiana 70803

A 17-reaction mechanism model was postulated to describe the alkylation of isobutane with propylene using sulfuric acid as the catalyst. The scheme was based on the Schmerling carbonium ion mechanism with modifications introduced to account for iC_9 and iC_{10} formation. Solving the steady state rate equations for the rate constants a set of 17 equations of the form $k_i = f(rC_j, rC_k, \ldots)/g\,(C_i, C_k, \ldots)$ were obtained. Experimental measurements were made in an ideally mixed, continuous-flow stirred-tank reactor, and the necessary data were obtained to compute the rate constants from 65°F to 135°F. The reaction model was found to be valid in the range of 81°F to 135°F using a 95% sulfuric acid catalyst since the rate constants obeyed the Arrhenius theory. The results obtained at 65°F and 95% sulfuric acid showed significant departure from the model. This was possibly due to a change in reaction mechanism. There was an apparent change in selectivity of the catalyst when the concentration was lowered to 90% sulfuric acid. This resulted in increased rates of formation of iC_9's and iC_{10}'s and decreased rates of formation of iC_5's, iC_6's and iC_8's.

The alkylation of a light isoparaffin with a light olefin in the presence of an aqueous phase catalyst has been the subject of extensive study. Investigations have studied both the effect of process variables on yield and product distribution (*1, 2, 5, 6, 9, 11, 14, 18, 19*) and the possible mechanisms of reactions (*4, 5, 7, 8, 10, 12, 15, 17, 19, 21, 22*). However, the kinetics of the reaction have remained largely unexplored. There appear to be two main reasons for this: (1). the presence of many competing reactions, and (2) two separate phases, hydrocarbon and aqueous. With the aqueous phase being the reaction medium, it is improbable that actual reactant and product concentrations can be measured.

This paper deals with a kinetic study of the alkylation of isobutane with propylene in the presence of a sulfuric acid catalyst. To circumvent problems mentioned above, a modified Schmerling mechanism has been used in conjunction with an analogous nonreacting system and mass transfer relations to derive the mathematical model.

Correspondence concerning this paper should be addressed to R. W. Pike. J. R. Langley is with Gulf General Atomic Inc., San Diego, California.

THEORY OF THE ALKYLATION MODEL

As Schmerling's mechanism (*7, 19*) is the most comprehensive one available, it served as the basis for the mathematical model used in this research. The mechanism for the isobutane-propylene reaction as presented by Schmerling describes possible routes of formation of C_3 through iC_8, iC_{10} and iC_{11} saturated hydrocarbon species; they are listed in Table 1. In this table modifications proposed by authors of later works such as Hofmann and Schriesheim (*4, 5*), Kennedy (*10*), and others (*16, 21, 22*) are also included. Specifically, the reaction to form the nonane fraction was a modification made in the light of the knowledge of Schmerling's and others' theories. This is Reaction (1-15) in Table 1. Also, the route of decane formation was tailored to account for the yields of this species over the temperature range investigated. The result is two reactions, one expressing formation of the decyl ion and one expressing its consumption. These are Reactions (1-13) and (1-17) respectively.

The formation of dimethyl-hexane via allylic ions as proposed by Hofmann and Schriesheim (*4, 5*) was considered a modification. However, as experimental information was lacking to discern between this theory and